Fusarium graminearum Ste3 g-protein coupled receptor: a mediator of hyphal chemotropism and pathogenesis

Sharma, Tanya; Sridhar, Pooja S.; Blackman, Christopher; Foote, Simon J.; Allingham, John S.; Subramaniam, Rajagopal; Loewen, Michele C.

Publisher's version / Version de l'éditeur:
https://doi.org/10.1128/msphere.00456-22
mSphere, 7, 6, 2022-11-15

AMERICAN SOCIETY FOR MICROBIOLOGY | mSphere®

RESEARCH ARTICLE

Fusarium graminearum Ste3 G-Protein Coupled Receptor: A Mediator of Hyphal Chemotropism and Pathogenesis

Tanya Sharma,[a,b] Pooja S. Sridhar,[c] Christopher Blackman,[d,e] Simon J. Foote,[f] John S. Allingham,[c] Rajagopal Subramaniam,[d,e] Michele C. Loewen[a,b,c]

[a]Department of Chemistry and Biomolecular Sciences, University of Ottawa, Ottawa, Ontario, Canada
[b]Aquatic and Crop Resources Development Research Center, National Research Council of Canada, Ottawa, Ontario, Canada
[c]Department of Biomedical and Molecular Science, Queen's University, Kingston, Ontario, Canada
[d]Department of Cell and Systems Biology, University of Toronto, Toronto, Ontario, Canada
[e]Agriculture and Agri-Food Canada, Ottawa, Ontario, Canada
[f]Human Health Therapeutics Research Center, National Research Council of Canada, Ottawa, Ontario, Canada

ABSTRACT Fungal hyphal chemotropism has been shown to be a major contributor to host-pathogen interactions. Previous studies on *Fusarium* species have highlighted the involvement of the Ste2 G-protein-coupled receptor (GPCR) in mediating polarized hyphal growth toward host-released peroxidase. Here, the role of the opposite mating type GPCR, Ste3, is characterized with respect to *Fusarium graminearum* chemotropism and pathogenicity. *Fgste3*Δ deletion strains were found to be compromised in the chemotropic response toward peroxidase, development of lesions on germinating wheat, and infection of *Arabidopsis thaliana* leaves. In the absence of *Fg*Ste3 or *Fg*Ste2, *F. graminearum* cells exposed to peroxidase showed no phosphorylation of the cell-wall integrity, mitogen-activated protein kinase pathway component Mgv1. In addition, transcriptomic gene expression profiling yielded a list of genes involved in cellular reorganization, cell wall remodeling, and infection-mediated responses that were differentially modulated by peroxidase when *Fg*Ste3 was present. Deletion of *Fg*Ste3 yielded the downregulation of genes associated with mycotoxin biosynthesis and appressorium development, compared to the wild-type strain, both in the presence of peroxidase. Together, these findings contribute to our understanding of the mechanism underlying fungal chemotropism and pathogenesis while raising the novel hypothesis that *Fg*Ste2 and *Fg*Ste3 are interdependent on each other for the mediation of the redirection of hyphal growth in response to host-derived peroxidase.

IMPORTANCE *Fusarium* head blight of wheat, caused by the filamentous fungus *Fusarium graminearum*, leads to devastating global food shortages and economic losses. Fungal hyphal chemotropism has been shown to be a major contributor to host-pathogen interactions. Here, the role of the opposite mating type GPCR, Ste3, is characterized with respect to *F. graminearum* chemotropism and pathogenicity. These findings contribute to our understanding of the mechanisms underlying fungal chemotropism and pathogenesis.

KEYWORDS hyphal chemotropism, *Fusarium graminearum*, Fusarium head blight, G-protein coupled receptors, wheat infection, pheromone receptor, wheat disease

In nature, fungi exist as sessile organisms that conduct spatiotemporal sensing and associated responses through their hyphae. Thus, their abilities to extend and control the trajectory of hyphal extension is tightly coordinated. A range of environmental cues control this hyphal behavior by either acting as a positive stimulus, encouraging hyphal growth, as seen in the case of nutrients, mating pheromones, and host signals, or acting as a negative stimulus, repelling the hyphae away as in the case of toxins (1). The phenomenon of polarized hyphal growth toward or away from external stimuli is

Editor Aaron P. Mitchell, University of Georgia

Address correspondence to Michele C. Loewen, Michele.Loewen@nrc-cnrc.gc.ca.

The authors declare no conflict of interest.

This paper represents National Research Council of Canada Communication no. 38345.

Received 14 September 2022
Accepted 19 October 2022
Published 15 November 2022

referred to as chemotropism, and is quintessential to fungal symbiotic, parasitic, and host-pathogen interactions.

A classic example of fungal chemotropism lies in the process of mating between *MATa* and *MAT*α cell types in model organisms, such as *Saccharomyces cerevisiae* and *Neurospora crassa*, which highlights growth toward a pheromone gradient (2–9). Similarly, the chemotropic responses of hyphae to nutrient sources were also demonstrated in several saprophytic and parasitic oomycetes fungi (10–12). However, evidence of hyphal chemotropism in phytopathogenic fungi is relatively sparse. Some of the earliest reports were in the phytopathogen *Cochliobolus sativus*, which exhibited preferential growth toward barley roots (13). Others demonstrated that when located adjacent to their host roots, *Phytophthora cinnamoni* cysts germinated rapidly and grew in the direction of the roots (14). More recently, researchers showed that soilborne *Fusarium oxysporum* displayed positive chemotropic growth toward catalytically active class III peroxidases that were released by host tomato roots (15).

With respect to the molecular machinery mediating hyphal chemotropism, G-protein coupled receptors (GPCRs) have been shown to play a critical role (16–18). Characterized by their cell membrane localization and seven transmembrane domain structure, GPCRs classically function as molecular switches at which the binding of an external ligand elicits conformational changes in the receptor that lead to the dissociation of intracellular heterotrimeric G-proteins with a corresponding exchange of GDP to GTP on the G-α subunit (19). The released G-protein domains activate downstream signaling cascades, leading to the activation of various cellular responses. In the model system *S. cerevisiae*, the diffusible α-factor and a-factor pheromones bind their respective *Sc*Ste2p and *Sc*Ste3p receptors to mediate mating in a paracrine fashion (20, 21). The stimulation of these receptors activates the filamentous growth mitogen-activated protein kinase (MAPK) pathway (Ste11p, Ste7p, Fus3p, and Ste12p), thereby yielding physiological changes in each mating cell type and leading to cell cycle arrest and shmoo formation (3–9). A cooperative role for *Sc*Ste2p and *Sc*Ste3p in subsequent zygote development has also been proposed (2). In *F. oxysporum*, receptors *Fo*Ste2 and *Fo*Ste3 have been shown to be stimulated by pheromones in an autocrine fashion to control conidial germination in a density-dependent manner (22). High concentrations of the α-factor repress germination, but when Bar1 protease is secreted from the cells, it cleaves the α-factor, thereby increasing the relative concentration of the a-factor and relieving the repression.

Interestingly, Ste2 was recently shown to be responsible for perceiving and transmitting the peroxidase-mediated chemotropic responses in *F. oxysporum*, *F. graminearum*, and *Verticillium dahliae*, underscoring the general relevance of this GPCR in chemotropism (15, 23, 24). The deletion of Ste2 also led to a decrease in the virulence of these pathogens on their known hosts, including tomato roots, germinating wheat coleoptiles, and eggplant seedlings. The peroxidase-stimulated response in *Fusarium* and *Verticillium* species was shown to be transduced by the highly conserved cell wall integrity (CWI) MAPK pathway (15, 23, 24). Deletion mutants lacking genes integral to the CWI pathway, including Rho1, Bck1, Mkk2, and Mgv1 (Mpk1; Slt2) were impaired in peroxidase-mediated chemotropism. This is in contrast to genes belonging to the filamentous growth MAPK pathway, including Ste11, Ste7, Gpmk1 (Fmk1; Fus3), and Ste12, the deletion of which had no impact on peroxidase-mediated chemotropism. In addition to chemosensing, the CWI pathway has been implicated in pathogenesis by promoting infection and penetration through appressorium formation, the osmotic stress response, and deoxynivalenol (DON) biosynthesis (25–27).

The prior observation of synergistic relationships between Ste2 and its cognate pheromone receptor Ste3 raised the novel hypothesis that Ste3 may also play a role in host sensing. To address this, the chemotropic and virulence potential of *STE3* was explored through a reverse genetic approach, using a CRISPR-generated *FgSTE3* deletion mutant. Downstream signaling pathway activation and transcriptomic studies revealed the functional relevance and mechanistic aspects underlying the observed chemotropic responses to host peroxidase and associated pathogenesis.

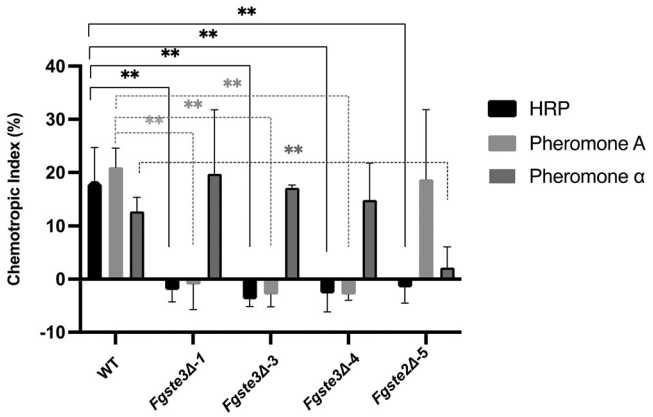

FIG 1 *F. graminearum* chemotropic growth toward peroxidase is mediated by both Ste3 and Ste2 receptors. Polarized hyphal growth of wild-type, *Fgste3Δ-1*, *Fgste3Δ-3*, *Fgste3Δ-4*, and *Fgste2Δ-5* were calculated 12 h after exposure to the indicated chemoattractants. Hyphae growing toward either 4 μM horseradish peroxidase (HRP), pheromones a-factor or α-factor (378 μM) were counted against a competing solvent control gradient (water or 50% vol/vol methanol, respectively). Data are representative of averages of 3 independent replicates (n = 500 hyphae/interaction/replicate; **, $P < 0.001$). Error bars represent the standard deviation. The statistics were assessed using Student's t test.

RESULTS

Deletion of *F. graminearum STE3* compromises chemotropism toward peroxidase. To determine whether *Fg*Ste3 is involved in mediating the chemotropic response to peroxidase, the annotated *F. graminearum STE3* gene sequence (*FGSG_07270* [28–30]) was deleted from *F. graminearum*. A CRISPR-CAS9-mediated transformation strategy was applied using a homology-directed repair mechanism, in which the entire *FgSTE3* open reading frame was replaced with a hygromycin-resistance gene cassette (Fig. S1). Hygromycin-resistant transformants were isolated (*Fgste3Δ-1*, *Fgste3Δ-2*, *Fgste3Δ-3*, and *Fgste3Δ-4*) and validated via polymerase chain reaction (PCR) amplification, using primers specific to the *FgSTE3* gene (Fig. S2). Sanger sequencing was performed on the obtained strains, and whole-genome sequencing was performed on strain *Fgste3Δ-3*, validating the insertion and confirming that the observed phenotype was exclusively due to the loss of *FgSTE3*, with no off-target effects.

The three positive *FgSTE3* deletion knockout strains were subjected to chemotropism plate assays and were screened against commercially available peroxidase (horseradish peroxidase [HRP]) (Fig. 1). The wild-type strain was assayed as a positive chemotropic control, and the previously characterized *Fgste2Δ-5* was also included for comparison and as a negative control (24). All three *Fgste3Δ* strains consistently showed random hyphal growth in the presence of HRP, compared to the directed growth observed for the wild-type strain. This indicates that the chemotropic response to HRP was completely abolished with the deletion of *FgSTE3*. Chemotropism of the wild-type strain was fully characterized again for the hyphal length, angle of hyphal growth, and sensitivity of the activity to active peroxidase, with the obtained values being consistent with those of its prior characterization in our previous work (Fig. S3A–C) (Sridhar et al., 2020 [24]).

Deletion of *FgSTE2* or *FgSTE3* does not affect pheromone-induced chemotropism arising from the remaining opposite pheromone receptor. The chemotropic preferences of *Fgste2Δ* or *Fgste3Δ* strains toward *F. graminearum* pheromones were also investigated. Hyphae growing toward either *F. graminearum* a-factor or α-factor pheromones were quantified compared to those of the wild-type (Fig. 1). While the wild-type showed a strong response toward both pheromones, the *Fgste3Δ* strains had no response to the a-factor, consistent with the absence of *Fg*Ste3. However, the chemotropic response to the α-factor was retained, consistent with the native expression of *FgSTE2* in these deletion strains. Similarly, the *Fgste2Δ-5* strain showed no chemotropic response to the *Fg*Ste2 α-factor pheromone, but it retained its response to the *Fg*Ste3 a-factor pheromone. Overall, the responses of these strains to pheromones differ from their responses to HRP, where all responses to HRP were lost, regardless of which receptor was deleted (Fig. 1).

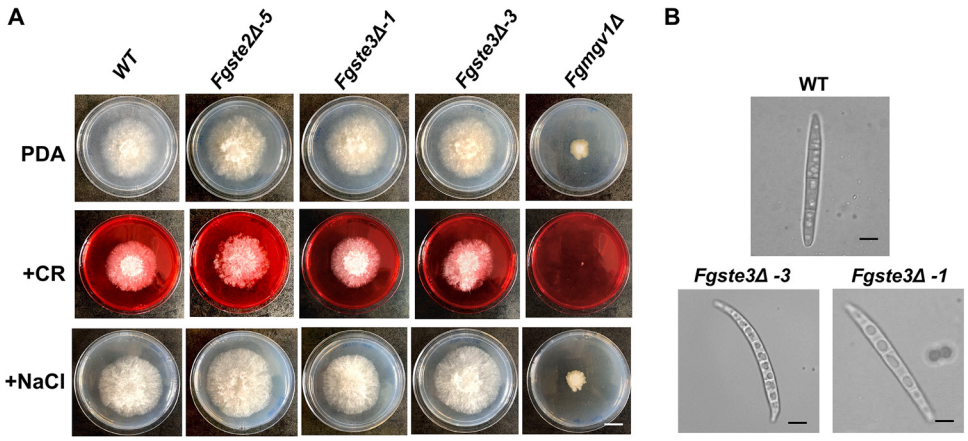

FIG 2 *FgSTE3* deletion has no effect on *F. graminearum* morphology or on osmotic stress tolerance. (A) Images of wild-type and mutant strains *Fgste2*Δ*-5*, *Fgste3*Δ*-1*, *Fgste3*Δ*-3*, and *Fgmgv1*Δ conidia grown on PDA, Congo red (CR; 150 μg/mL), and NaCl (0.7 M). Similar results were obtained for two independent experiments. Size bar = 1 cm. (B) Conidia for the wild-type, *Fgste3*Δ*-3* and *Fgste3*Δ*-1* were imaged under 100× using oil immersion. The images were captured using cellSens software, version 1.12. Size bar = 10 μM.

This finding suggests that different receptor mechanisms underlie the perception of the pheromones versus the HRP signal.

***FgSTE3* deletion has no effect on cell wall stress responses or osmotic stress tolerance.** Initial observations of colony growth indicated no significant differences in the growth pattern, colony color, or morphology of the *Fgste3*Δ strains, compared to the wild-type strain or the *Fgste2*Δ*-5* strain. They all displayed normal growth with no visible change in the presence of Congo red (cell wall stressor) or NaCl (an osmotic stressor), respectively (Fig. 2A). Microscopic examination showed that the *Fgste3*Δ*-3* and *Fgste3*Δ*-1* conidia were slightly longer and narrower, compared to those of the wild-type (Fig. 2B).

***FgSTE3* deletion leads to decreased virulence and pathogenicity.** To further investigate whether *Fg*Ste3 is involved in mediating fungal pathogenesis, a coleoptile infection assay was performed on the wild-type and *Fgste3*Δ*-3* strains. This assay has been shown to be an effective, reliable, and easily quantifiable method to investigate the pathogenicity and extent of *Fusarium* head blight infection (24, 31). The *Fgste3*Δ*-3* strain showed an average 50% decrease in lesion length compared to the wild-type strain (Fig. 3A and B). This trend is consistent with results arising from an *A. thaliana* leaf infection assay, in which decreased lesions for *Fgste3*Δ*-3* were observed, compared to the wild-type strain (Fig. 4A and B). A quantitative polymerase chain reaction (qPCR) analysis for fungal biomass quantification in the *A. thaliana* assay showed a 50% decrease in the absence of *Fg*Ste2 and a 99% reduction in the absence of *Fg*Ste3 (Fig. 4C). In the case of *Fg*Ste3 deletion, the fact that such a small amount of pathogen could elicit the observed lesion at all supports the claim that many of the lesions arise from host-mediated responses, leading to cell death.

Consistent with this, investigations of pathogenesis on flowering wheat heads yielded a decrease in percent infected spikelets for both the *Fgste3*Δ and *Fgste2*Δ deletion mutants (Fig. S4A), although these differences were not deemed statistically significant, compared to the wild-type under the conditions tested. The production of the mycotoxin DON, a *Fusarium* virulence factor and a critical component in fungal infections on wheat (32), was also assessed for the deletion mutants. Extracts were taken from suspension cultures of the wild-type, *Fgste3*Δ, and *Fgste2*Δ deletion strains grown on a medium that induces production of trichothecenes. Consistent with the wheat head infection results, both deletion mutants produced lower levels of DON, on average (Fig. S4B), with *Fgste3*Δ*-3* yielding a reduction of 30%, compared to the wild-type. The *P* value was slightly above the statistical significance cutoff ($P = 0.069$).

Activation of the CWI-MAPK pathway by peroxidase is mediated by *Fg*Ste3 and *Fg*Ste2. It has previously been shown that the presence of peroxidase activates the CWI-MAPK pathway in *F. graminearum* (24). However, the roles of *Fg*Ste3 and *Fg*Ste2 in

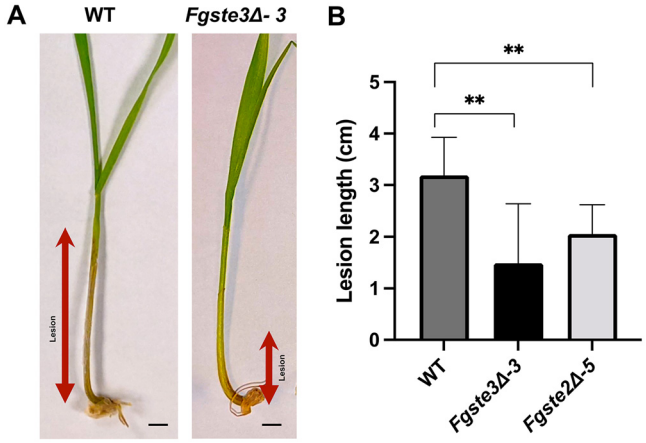

FIG 3 Deletion of *FgSTE3* leads to decreased *F. graminearum* pathogenicity against wheat. (A) The pathogenicity was quantified via the measurement of the length of infected stalk or lesion formed on germinating "Roblin" coleoptiles that were infected with the indicated *F. graminearum* strains. Shown are representations of lesions formed around the wound site 10 days after infection with *F. graminearum* conidia. (B) Quantification of average lesion length formed on germinating "Roblin" coleoptile stalks infected with *F. graminearum* wild-type and mutant strains *Fgste3*Δ*-3* and *Fgste2*Δ*-5*. The averages of two representative experiments are shown (compared to the wild-type strain; $n = 18$; **, $P < 0.005$). Error bars represent the standard deviation. The statistics were assessed via Student's *t* test. Size bar = 1 cm.

transducing this signal across the membrane to the CWI-MAPK have not been tested. Here, the phosphorylation of the CWI-MAPK pathway component Mgv1 was assayed using the phospho-p44/42 antibody in the presence and absence of *Fg*Ste3 or *Fg*Ste2. The phosphorylation of Mgv1 (expected molecular weight [MW] of 47 kDa) showed a 3-fold decrease in both mutants, compared to the wild-type (Fig. 5A and B; Fig. S5). Gpmk1 (expected MW of 41 kDa; MAP kinase in the filamentous signaling pathway that is also detectable by the phospho-p44/42 antibody [24]) was not detected using the phospho-p44/42 antibody. However, neither of the relative total amounts of Mgv1 or Gpmk1 varied from the wild-type levels in the knockout strains when probed with

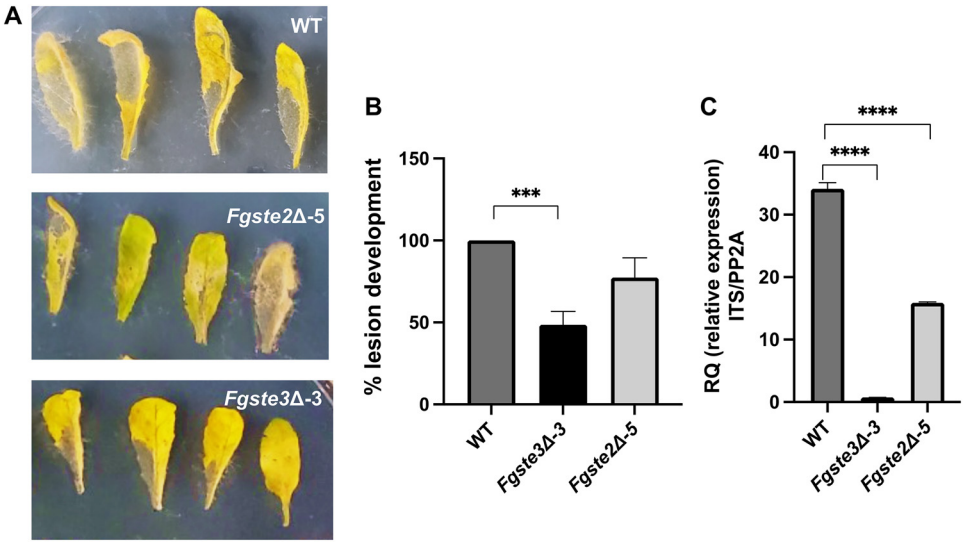

FIG 4 Deletion of *FgSTE3* leads to decreased *F. graminearum* pathogenicity against *A. thaliana*. (A) Representative images of *A. thaliana* leaf infected with *F. graminearum* strains. (B) Assessment of lesion development on *A. thaliana* leaves. Leaves were infected with the wild-type, *Fgste3*Δ*-3*, and *Fgste2*Δ*-5* strains and quantified 3 days postinfection using Image J software. (C) Assessment of *F. graminearum* infection via quantitative PCR. Quantitative PCR was performed with genomic DNA isolated from Arabidopsis leaves infected with the wild-type, *Fgste3*Δ*-3*, or *Fgste2*Δ*-5* strain. The relative expression (RQ) was measured with the *Fusarium ITS2*, with respect to the Arabidopsis *PP2A*. The experiment was performed three times (three biological replicates with $n = 12$ for each) with similar results. Error bars denote the standard deviation. The statistical analysis was performed using Student's *t* test (****, $P < 0.0005$). Size bar = 1 cm.

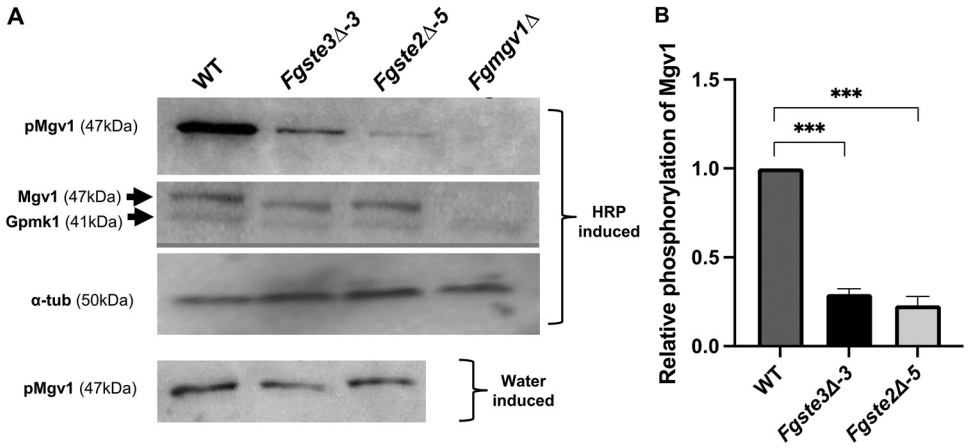

FIG 5 Activation of the CWI-MAPK pathway by peroxidase is mediated by *Fg*Ste3 and *Fg*Ste2. (A) Representative images of a quantitative Western blot to probe CWI pathway activation by tracking the phosphorylation of Mgv1 and total MAPK isolated from wild-type and mutant strains *Fgste3Δ-3*, *Fgste2Δ-5*, and *Fgmgv1Δ*. The conidia were grown for 48 h in regular PDB culture and were treated with commercially available HRP or a water control for 1 h before total protein extraction. For the normalization of the quantification, α-tubulin was probed. The molecular weights of the detected proteins are indicated on the blot. (B) The intensity of phospho-Mgv1 was quantified and normalized to tubulin, with relative intensities compared to the wild-type (***, $P < 0.0005$). Quantification analysis was performed using ImageJ software. The data represent averages of three independent experiments. Error bars represent the standard deviation. The statistical analysis performed using Student's *t* test.

the total p44/42 antibody or with the water control. The *Fgmgv1Δ* strain served as a negative control and validated the detected 47 kDa band as Mgv1. These results indicate that the deletion of either *FgSTE3* or *FgSTE2* individually decreases the phosphorylation of Mgv1 to some extent, compared to the wild-type.

Comparative transcriptomic analysis of the regulation of *F. graminearum* gene expression by peroxidase and *Fg*Ste3. RNA-Seq reads were mapped to the genomic sequence of *F. graminearum*, resulting in 99.3% of the reads being successfully mapped. The different strains and treatments analyzed resulted in limited distinguishable changes to the transcriptome (Fig. 6A). After the normalization of the read counts, a total of 383 differentially expressed genes (DEGs) were identified for three pairwise comparisons relevant to this analysis, based on adjusted *P* values of ≤0.05 (Table 1; Data Set S1). The bulk (96.9%) of the DEGs arose from the comparison of the wild-type strain in the presence and absence of HRP. Consistent with this, the transcriptomic responses were most clearly divided based on the presence or absence of HRP and

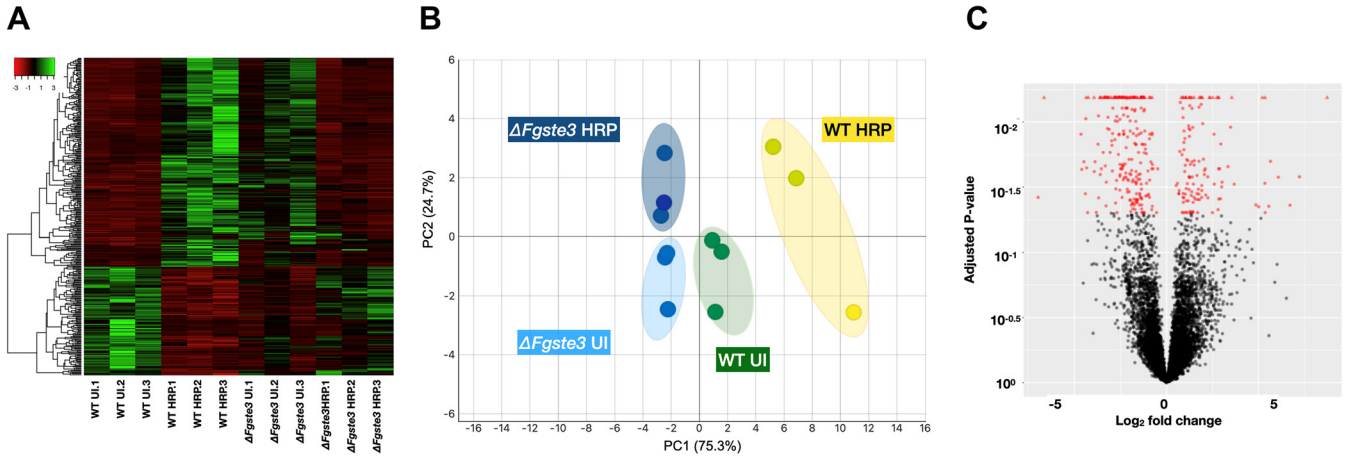

FIG 6 Transcriptomic overview of *F. graminearum* responses in the presence and absence of peroxidase and *Fg*Ste3. (A) Heat map showing the differential gene expression for different strains and conditions highlighting varying levels of upregulation and downregulation. (B) PCA plot showing the clustering of three biological replicates for each representative condition. (C) Volcano plot showing upregulated responses in the wild-type + HRP versus the wild-type uninduced pairwise comparison.

TABLE 1 Total numbers of DEGs upregulated or downregulated arising from each pairwise comparison considered in this study

DEG regulation	Pairwise comparison		
	Wild-type + HRP/ wild-type uninduced	*Fgste3*Δ*-3* + HRP/ wild-type + HRP	*Fgste3*Δ*-3* uninduced/ wild-type uninduced
Up	127	4	1
Down	243	4	4

were found to be contributing 75.3% of the variance in a principal components analysis (PCA) (Fig. 6B).

Comparison 1: wild-type F. graminearum in the presence versus the absence of HRP.

The pairwise comparison of the DEGs from the wild-type strain in the presence and absence of HRP was investigated to obtain broader insight into the genes potentially contributing to the HRP-induced chemotropic response in *F. graminearum*. While almost twice as many genes were downregulated as were upregulated (Table 1; Fig. 6A), a volcano plot analysis of the DEGs emphasizes the stronger nature of the upregulated responses (Fig. 6C). This is consistent with the idea of HRP inducing significantly increased expression of elements required to elicit chemotropism. Thus, the focus of this particular analysis is on the upregulated genes.

A gene ontology analysis of the upregulated genes highlighted the significant modulation of integral membrane transport activity (Table 2). *F. graminearum* is well-known

TABLE 2 List of genes upregulated in the wild-type + HRP versus wild-type uninduced comparison

Gene identifier	Description	log_2-fold change	*P* value
Membrane transporters			
FGSG_13980	The Major Facilitator Superfamily (MFS)	40.473	0.0008059030136
FGSG_07502	Transmembrane amino acid transporter	32.113	0.001594424155
FGSG_05731	Major Facilitator Superfamily transporter	11.643	2.43E−05
FGSG_00195	Monocarboxylate transporter 2	6.029	0.0008284057597
FGSG_04217	Pantothenate transporter liz1	5.969	0.0001984533517
FGSG_04426	Major Facilitator Superfamily transporter	2.853	0.0003898785871
FGSG_04095	Na(+)/H(+) antiporter 1	2.609	0.0004091487212
FGSG_00924	The Major Facilitator Superfamily	2.394	0.0006870875037
Cell wall remodeling			
FGSG_03616	6-hydroxy-D-nicotine oxidase	46.812	0.001572254889
FGSG_03925	Alpha/beta hydrolases	40.945	0.001858777969
FGSG_13343	NBD_sugar-kinase_HSP70_actin	7.06	1.70E−05
FGSG_00659	Endoplasmic reticulum mannosyl-oligosaccharide -alpha-mannosidase	2.446	0.001764702055
Pathogenesis			
FGSG_01586	Retinol dehydrogenase 14	4.152	0.0006120705837
FGSG_11438	Ankyrin repeat	3.148	0.0006318247356
FGSG_04314	ATP-dependent Clp protease ATP-binding subunit	2.829	0.0004512020458
FGSG_07493	Sensor gacS	2.328	0.0009534158274
FGSG_05147	Putative SCRAMM family adhesin clumping factor ClfB	2.111	0.001365630372
Peroxisomes			
FGSG_07104	Peroxisome biosynthesis	2.398	8.06E−05
FGSG_00724	Peroxisomal biogenesis factor 2	2.028	0.001092628833
FGSG_05596	Peroxisomal biogenesis factor 6	1.866	0.001059428996
FGSG_01174	Peroxisomal targeting signal receptor	1.677	7.47E−05
Mitochondria			
FGSG_12693	Altered inheritance of mitochondria 32	7.087	0.0005160525821
FGSG_01639	Enoyl-delta isomerase mitochondrial	2.685	0.0001528329539
FGSG_05197	Fmp40 found in mitochondrial proteome	2.611	9.19E−05
FGSG_11231	MOSC mitochondrial	2.073	2.44E−05

to employ transporters to pump out the DON mycotoxin that it produces, depositing it on host cells (33). Major Facilitator Transporters are also known to act as energy centers that obtain nutrition that the pathogen needs for its survival (34). The best representative hits here include one of the top 10 most highly upregulated genes, the Major Facilitator Superfamily (MFS) transporter, *FGSG_13980*, although its function is not clearly defined (Table 2). Also notable is the significant upregulation of the MFS family pantothenate transporter Liz1 (*FGSG_04217*), which is known to contribute to septa formation and cellular development. Mutants of this gene have been shown to be defective in cell elongation and cell division in *S. pombe* (35).

With relevance to chemotropism, a wider variety of genes and their homologues involved in cellular development and cell wall organization are highlighted (Table 2). The upregulation of hippurate and alpha/beta hydrolases (*FGSG_03925*), which are known to be involved in cell wall remodeling in fungi, was detected (36). In addition, alpha-mannosidase (*FGSG_00659*), which is required for the synthesis of mannose rich-N-glycans and is one of the major constituents of cell wall biosynthesis in rapidly dividing cells, was also upregulated (37). The upregulation of NBD sugar-kinase HSP70 actin (*FGSG_13343*), which regulates the formation of actin filaments in cells, was noted (38). Finally, and perhaps most clearly related to chemotropism at this time, was the observed upregulation of 6-hydroxy-D-nicotine oxidase (*FGSG_03616*), which is involved in the production of hydrogen peroxide. In *F. oxysporum*, hydrogen peroxide has been shown to be directly involved in mediating peroxidase-stimulated hyphal chemotropism, based on its biosynthesis by the nicotinamide adenine dinucleotide phosphate (NADPH) oxidase (NOX) gene (39).

Further investigation of the DEGs revealed additional hits with more direct relevance to infection mechanisms but less potential relevance to chemotropism. These include the upregulation of the gene *FGSG_05147*, which is related to the SCRAMM family adhesin clumping factor ClfB. It is used primarily by bacterial species such as *Staphylococcus* to promote the attachment and invasion of host cells. A protein that contains ankyrin repeats (*FGSG_11438*) is required for host-mediated nitric oxide production, and is known to promote virulence in *F. graminearum* was also upregulated (40). The upregulation of the gene *FGSG_04314* was also notable. It shares 36% identity with a homologue of Clp protease, an ATP-binding subunit adaptor protein that is known to be involved in the regulation of virulence genes in *S. aureus*, and 39% identity with a homologue of ClpX in *S. cerevisiae* (Mcx1p), which is known to act as a molecular chaperone that contributes to thermotolerance (41–43). Also upregulated was *FGSG_07493*, related to the putative gacS sensor, which is known to be involved in the control of the production of secondary metabolites and extracellular enzymes involved in pathogenicity in *Pseudomonas*. In addition, it mediates the production of acyl-homoserine lactones, which are responsible for quorum sensing in bacteria (44, 45). Though quorum sensing in pathogenic fungi has not been extensively studied, this raises a novel hypothesis that HRP may be involved in initiating the transcription of genes that enable fungal communication. *FGSG_07493* also shares 90% identity with *S. cerevisiae* nik-1, which is known to interact with Cdc28 and to regulate the progression of the cell cycle (46). Finally, retinol dehydrogenase (*FGSG_01586*), which is known to oxidise retinol to retinal (a precursor for carotenoid biosynthesis and abscisic acid [ABA] production), was also upregulated (47–49). The ABA phytohormone is well-known to act as a fungal effector and to accentuate fungal disease severity.

Four peroxisomal genes were identified as upregulated, including a peroxisomal targeting signal receptor (*FGSG_01174*), peroxisome biosynthesis factor 2 (*FGSG_00724*), a protein involved in peroxisome biosynthesis (*FGSG_07104*) and peroxisomal biogenesis factor 4 (*FGSG_05596*). Peroxisomes have been implicated as critical regulators of pathogenicity in *Fusarium*, harboring glutathione transferases that aid in the detoxification of host-derived proteins and in the maintenance of redox homeostasis. This highlights a possible mechanism for peroxide detoxification that is employed by *Fusarium* to deal with oxidative stress (50). Peroxisomes also control secondary metabolism involving DON biosynthesis, siderophore biosynthesis, and cell wall integrity in fungi (51).

TABLE 3 List of differentially expressed genes in the *Fgste3*Δ + HRP versus wild-type + HRP comparison

Gene identifier	Description	log_2-fold change	*P* value
Downregulated			
FGSG_12829	Hypothetical protein	−4.828	6.09E−06
FGSG_04590	Averantin oxidoreductase	−2.094	1.60E−06
FGSG_04596	O-methyl transferase B	−1.877	3.13E−05
FGSG_05039	*Putative PTH 11*	*−0.959*	*0.1623589568*
Upregulated			
FGSG_06536	L-pipecolate oxidase	7.003	4.92E−06
FGSG_09354	N amino acid transport system protein	5.936	1.66E−05
FGSG_09118	Hypothetical protein	5.469	1.59E−05
FGSG_09001	Transcription factor	1.543	1.03E−05

A variety of mitochondrial genes were upregulated, including the mitochondrial amidoxime-reducing component 1 (MOSC1; *FGSG_11231*) and the altered inheritance of mitochondria 32 (AIM32; *FGSG_12693*), the latter being a 2Fe-2S protein that functions in redox quality control (52). Additionally, two mitochondrial carrier proteins: Fmp40 (*FGSG_05197*), which is found in the mitochondrial proteome, and enoyl delta isomerase (*FGSG_01639*) were both upregulated. Although it is hard to predict in which morphogenetic changes these mitochondrial proteins might be involved, they are generally related to oxidative stress responses, based on mitochondria being major centers for the generation of hydrogen peroxide and reactive oxygen species (ROS), which are later taken up by the peroxisome. However, mitochondrial proteins have also been shown to directly influence fungal pathogenicity through phenotypic changes that involve cell wall modification, polysaccharide capsule modulation, the evasion of the host immune response, metabolic flexibility by alternating between carbon source utilization, and controlling cAMP/PKA signaling (53, 54).

Finally, gene enrichment analyses in Blast2GO and KOBAS (Fig. S6) highlighted significantly upregulated genes (enrichment ratio of 0.27) that are involved in the biosynthesis of the branched chain amino acids (BCAA) valine, leucine, and isoleucine. BCAAs have been shown to play important roles during *Fusarium* pathogenesis, with the mutants of genes specifically involved in leucine biosynthesis, such as *Fg*LEU2, *Fg*ILV2, and *Fg*ILV6, being attenuated in infection potential, conidiation, and mycelial development (55, 56). Gene enrichment further revealed that biologically, the majority of DEGs are associated with membrane transport, transcription by RNA pol II, carbohydrate metabolic processes, proteolysis, and cellular amino acid metabolic processes. With respect to molecular function, most DEGs fall into the oxidoreductase category/class, followed by hydrolases and nucleotide-binding.

*Comparison 2: Fgste3*Δ*-3 strain versus the wild-type strain, both treated with HRP.*

The pairwise comparison of the effect of HRP in the presence and absence of *FgSTE3* was assessed to gain insight into the role of *Fg*Ste3 in mediating transcriptomic changes in *F. graminearum* cells exposed to peroxidase, and, ultimately, the mechanism underlying *Fg*Ste3's regulation of chemotropism. Interestingly, only 8 DEGs were deemed significant in this comparison, based on our cutoff criteria (Table 3).

Significantly downregulated genes included two genes related to the production of fungal toxins during the infection process, including a sterigmatocystin 8-O-methyltransferase (*FGSG_04596*) and a gene related to isotrichodermin C15 hydroxylase (*FGSG_04590*), a cytochrome P450 monooxygenase CYP65A1 which has been previously described to be a part of a C16 gene cluster that is involved in terpenoid biosynthesis. The expression of these two genes has been shown to increase dramatically 72 h postinoculation (hpi) on barley and wheat, and thus, they play essential roles in plant infection (57).

Also notable is the downregulation of *FGSG_05039*, which shares 79% amino acid identity to a PTH11-like GPCR from *Hypocrea virens* (*Trichoderma*). PTH11 (*MGG_05871*)

TABLE 4 List of differentially expressed genes in *Fgste3*Δ *uninduced vs wild-type uninduced* comparison

Gene identifier	Description	log_2-fold change	*P* value
Downregulated			
FGSG_12651	Conserved hypothetical protein	−4.068	5.77E−06
FGSG_11101	Hypothetical protein	−3.215	7.25E−06
FGSG_08852	Putative cryptochrome DASH	−2.474	6.23E−08
FGSG_04576	Conidial development transcriptional regulator fluffy	−1.033	3.35E−06
Upregulated			
FGSG_01936	Cutinase transcription factor 1 alpha	0.663	2.39E−05

from *M. oryzae* is known to be involved in appressorium formation, contributing to the generation of turgor pressure and the entry of fungal hyphae into the cells, which potentially implicates HRP-stimulated *Fg*Ste3 directly in pathogenesis (58). Although the log_2-fold change was barely 1.0 for this hit, and although its adjusted *P* value was above the cutoff (Data Set S1), it shows a consistent decrease in all replicates. GPCRs are generally expressed at low levels, making their transcriptional detection challenging (59). For instance, even though *FgSTE3* was knocked out of the *Fgste3*Δ*-3* strain, because of its low constitutive expression in the wild-type strain, it did not fulfill the cutoff criteria that was set for this transcriptomic analysis and was not considered to be a downregulated gene, compared to the wild-type.

Of the upregulated genes, only L-pipecolate oxidase (*FGSG_06536*) was noted as an enzyme that was linked to lysine catabolism and protection against hydrogen peroxide stress (60). Thus, ultimately, while this pairwise comparison provides additional information regarding the potential regulatory roles of activated *FgSTE3* in infection, little insight was gained regarding the mechanism underlying its role in chemotropism.

*Comparison 3: Fgste3*Δ*-3 strain versus the wild-type strain, both untreated.*

Finally, the pairwise comparison of *Fgste3*Δ*-3* to the wild-type strain in the absence of any treatment was assessed to obtain further insight into the constitutive role of *Fg*Ste3. Constitutive activity refers to any basal level of signaling activity that a GPCR elicits in the absence of ligand stimulation. Many GPCRs are well-known to elicit constitutive activity (61). However, based on the cutoff criteria, only 5 genes were shown to be significantly differentially regulated upon the deletion of *Fg*Ste3 (Table 4), suggesting that *Fg*Ste3 has minimal, if any, constitutive role under these assay conditions.

Nonetheless, the one upregulated gene in the *Fgste3*Δ*-3* strain (albeit with a log_2-fold change of only 0.6) was the cutinase transcription factor 1-α (*FGSG_01936*), which has been shown to be dispensable in *F. oxysporum* virulence (62). Thus, the relevance of the repression of this gene by constitutive *FgSTE3* remains enigmatic. With respect to the few downregulated hits detected, *FGSG_04576* is a homologue of the major regulator of conidiation in *Neurospora crassa* and is known as Fluffy. Fluffy is also known to directly activate a developmentally-regulated hydrophobin gene that is involved in osmotic stress tolerance (63). Finally, a gene related to the putative *Drosophila*, *Arabidopsis*, *Synechocystis*, human (DASH) cryptochrome (*FGSG_08852*), which is known to be involved in DNA photorepair and in the regulation of conidiation in the gray mold fungus *Botrytis cinerea* (64, 65), was also downregulated. Together, these results point toward a limited role for constitutive *Fg*Ste3 in stress sensing and in the regulation of conidiation and photoreception, although these findings remain to be validated functionally.

DISCUSSION

F. graminearum is an aggressive pathogen of cereal crops that continues to adapt to the current line of antifungal agents (66). Prior studies emphasized dual roles for Ste2 and Ste3 in many of the biological processes that they regulate across fungal species (2–9, 22). The present study lends further evidence to this, demonstrating the

involvement of the *Fg*Ste3 receptor in mediating chemotropism toward host-secreted peroxidases and virulence in its host, similar to activities previously documented for the opposite mating type receptors *Fg*Ste2, *Fo*Ste2, and *Vd*Ste2 (15, 23, 24).

The underlying mechanisms mediating the chemotropic responses for either *Fg*Ste2 or *Fg*Ste3 remain somewhat enigmatic. Previously, peroxidase induction of the CWI-MAPK pathway was demonstrated for *F. graminearum*, *F. oxysporum*, and *V. dahliae* (15, 23, 24). Here, this was extended by confirming the involvement of *Fg*Ste2 and *Fg*Ste3 in mediating this signal from peroxidase to Mgv1 in the CWI-MAPK pathway, with observed decreases in Mgv1 phosphorylation for both peroxidase-stimulated mutant strains (Fig. 5). With Mgv1 previously being shown to be important in fungal hyphal growth and pathogenicity (67, 68), these results are consistent with the observed reduction in chemotropic responses (Fig. 1) (24).

Further consideration of the chemotropic results emphasizes that the responsiveness of this homothallic *F. graminearum* fungus to pheromones is consistent with responses observed previously for the asexual *F. oxysporum* (22). This includes the observation that receptor deletion strains respond only to the opposite pheromone (Fig. 1). Furthermore, it is notable that each independent deletion is close to being fully effective in inhibiting peroxidase-directed chemotropism (Fig. 1). Because only one of the two pheromone receptors is deleted in each mutant strain, it follows that the remaining receptor is incapable of mediating the peroxidase-stimulated chemotropic response, even a partial one, on its own. That is to say that neither of the two receptors can compensate for the loss of the other receptor. This raises the novel hypothesis that *Fg*Ste2 and *Fg*Ste3 work together to mediate the chemotropic response to peroxidase. Speculatively, this interdependence may be the result of independent signaling events elicited by each individual receptor. In this case, one might expect that changes to the chemotropic responses would be cumulative, rather than absolute, with single receptor deletion. Additionally, in that both receptors stimulate the CWI pathway, the interdependence could be consistent with a requirement for the formation of a peroxidase-stimulated heterodimer complex between *Fg*Ste2 and *Fg*Ste3 in the cell membrane. GPCR dimers (hetero and homo), as well as higher order oligomers, are well-documented to play important roles in modifying GPCR signal transduction (69), including a prior report of Ste2p homooligomerization in yeast mating (70).

Host infection assays were used to assess the extent of fungal pathogenicity related to the *Fg*Ste3 receptor. Coleoptile infection data showed a consistent and significant decrease in lesion development, yielding a reduction of almost 50% compared to the wild-type (Fig. 3), similar to observations made previously for the *Fgste2*Δ strain (24). In contrast, slightly decreased values for the average infections of wheat heads and lower accumulations of DON for both *Fgste3*Δ*-3* and *Fgste2*Δ*-5* were not found to be statistically significant (Fig. S4). While confirming the contribution of *Fg*Ste3 to virulence, the comparison of results from wheat heads and wheat coleoptiles suggests that different routes of pathogenesis may be more or less reliant on *Fg*Ste2 and *Fg*Ste3 (i.e., potentially more prominent in stalk infections than in wheat head infections) (24). Additionally, in plants, salicyclic acid (SA) defense is generally predominant against biotrophic pathogens, and jasmonic acid and ethylene (JA/ET) allow resistance to necrotrophic pathogens. Both the SA and JA/ET defense responses can also attenuate each other or work in a synergistic way (71, 72). Thus, with *F. graminearum* being a hemi-biotroph, plants could elicit a wide range of variable defense responses that potentially differ in wheat head and coleoptile tissues. Alternatively, the difference between wheat head and coleoptile infection results may simply be a product of the assay systems. With the conidia being deposited directly at the site of infection on the kernel of a wheat head with a pipettor, any significant need for chemotropism may be eliminated. In contrast, the coleoptile assay sees the conidia presented to the leaf indirectly on cotton fibers dipped in conidia suspensions and then wrapped loosely around the wound sites. As such, chemotropism could be necessary for the hyphae to even make initial contact with the coleoptile leaf.

The results loosely linking DON accumulation to the pheromone receptors opens the question of the broader impact and role of *Fg*Ste3 in *F. graminearum* infection. To glean

further insight into the mechanisms related to peroxidase-induced, *Fg*Ste3-mediated chemotropism and virulence, a comparative transcriptomic study was completed. At the time of writing, this is the first global transcriptomic RNAseq study carried out in the context of the peroxidase-mediated chemotropism of *Fusarium*, to our knowledge. Broadly speaking, the DEG analysis highlighted a somewhat limited but fairly diverse array of modifications arising from treatment with peroxidase. Detailed DEG interpretations are largely included above in the Results section. However, more generally, with respect to oxidation and as a known component of the plant pathogen defense response (24, 49), it is not surprising that *F. graminearum* would have multiple varied responses to treatment with peroxidase. For example, transcription factors related to purine utilization and the cutinase enzyme used for plant cutin degradation were seen to be upregulated in the wild-type strain in response to peroxidase. As well, ornithine cyclodeaminase, which favors the conversion of ornithine to proline during the stress response was also upregulated. Notably, ornithine is an essential component in the synthesis of DON (73, 74).

With respect to chemotropism, HRP induced a selection of genes involved in cell wall remodeling and with relevance to hyphal redirection during growth. Many additional changes linked to pathogenic transitions that contribute to the switch from the benign phase to the beginning of the pathogenic phase, both for penetration and for obtaining nutrition, were also observed. Previous transcriptomic studies of *Fusarium* interactions with host plants have also highlighted the upregulation of peroxidases, which in turn activate other ROS-related genes. The expression of various pathogen associated molecular patterns (PAMPs) is also known to induce ROS bursts in host plants (75). In yeast, ROS stress is known to activate various signaling pathways and Rho GTPases, the guardians of the cell wall integrity pathway, with Rho1 controlling cell polarity (76).

In contrast, only a limited number of transcriptional changes were detected upon *Fg*Ste3 deletion. In the presence of HRP, genes involved in mycotoxin biosynthesis and appressorium formation were downregulated in the absence of *Fg*Ste3, linking important virulence-related events to this receptor. The fact that this transcriptomic analysis did not reveal a connection to chemotropic-related machinery, such as CWI pathway components or cell wall modifying enzymes, may be due to underlying mechanisms acting at the post-transcriptional level, generally low expression levels of signal transduction machinery, or strong general HRP effects masking the weaker Ste3-related mechanisms. Alternatively, the 24 h post HRP-induction time point selected for this transcriptomic analysis may not have been optimal for the detection of *Fg*Ste3-related events.

Overall, this report demonstrates a role for *Fg*Ste3 in chemotropism and virulence. This is consistent with previous reports that highlight similar roles for Ste2 (15, 23, 24). While the transcriptomic analysis shed only limited light on the mechanisms by which *Fg*Ste3 might be mediating chemotropism, a clear relationship between HRP stimulation and cell-wall remodeling is highlighted. As well, potential roles for *Fg*Ste3 in mycotoxin production and appressorium formation are noted. Finally, evidence that *Fg*Ste2 and *Fg*Ste3 are interdependent on each other for the perception of the peroxidase-derived signal and the elicitation of the chemotropic response is highlighted. Experiments investigating the interdependence of the receptors' roles in chemotropism, along with the elucidation of the nature of the peroxidase-derived ligand stimulating the receptors, are ongoing in our labs. Together, this research will enhance our understanding of how two related GPCRs can play so many different roles across mating, host perception, and virulence.

MATERIALS AND METHODS

Chemicals. All chemicals were obtained from Sigma-Aldrich (Burlington, MA, USA) unless otherwise indicated below.

Fungal strains, preparation of conidia and protoplast production. *F. graminearum* wild-type strain DAOM 233423 (also known as GZ 3639) was provided by C. Babcock of the Canadian Collection of Fungal Cultures (CCFC/DAOM), Agriculture and Agri-Food Canada, Ottawa. The *Fgste2Δ-5* deletion strain arose from wild-type GZ 3639, as did *Fgmgv1Δ*, and both are described in detail in our prior work (24). The wild-type strain was inoculated into 200 mL of liquid carboxymethylcellulose (CMC) media from a frozen glycerol stock and was grown in a rotating shaker at 180 rpm for 4 days at 28°C in the dark.

TABLE 5 List of primers and crRNA sequences

Name	Description	Sequence
P1[a]	5′ Hygromycin repair template	ATATATACTCAACCACTCACTCAAGAGCCTCAAAAAGCCTCTTCCACATC**TCGACAGAAGATGATATTG**
P2[a]	3′ Hygromycin repair template	AAAAAGGCACAAAAATCAAATAGGGTATCGCACGATGTACTTTTTGG**CCACTATTCCTTTGCCCTCGGACGA**
P3	Ste3 gene ORF-F	ATGGCCGATTCAATTCACTTG
P4	Ste3 gene ORF-R	CTAGCGTCGATATGTTTCCTC
P5	(*Fusarium*) ITS2 F	GTCGAGCTTCCATAGCGTAGTA
P6	(*Fusarium*) ITS2 R	CTACCTGATCCGAGGTCAACAT
P7	Arabidopsis PP2a (At 1G69960) F	AGTTCCAGAATCCAAACCAAC
P8	Arabidopsis PP2a (At 1G69960) R	CCTAGAGGCAACACAAACATC
C1	5′crRNA	AAAAAGCCTCTTCCACATCA
C2	3′crRNA	ATTCATCATCTATTCCGGGG

[a]The region in bold denotes hygromycin overlapping sequences.

Macroconidia were harvested by filtering the culture through a double layer of sterile cheesecloth, and this was followed by centrifugation for 10 min at 1,500 × *g* at 4°C. The supernatant was discarded, and the conidia were washed twice with sterile water and then resuspended to obtain a concentration of approximately 7×10^8 conidia per mL, as measured by a haemocytometer. For protoplast production, 1 mL of the conidia solution was inoculated into 100 mL of yeast peptone dextrose (YPD, BD Difco) media and grown for 8.5 h at 28°C with shaking at 170 rpm. When the germ tubes were observed to be approximately 1.5 times the length of the conidium, the mycelia were harvested by filtration through double layered Mira cloth and were washed with 50 mL of sterile water and 30 mL of 1.2 M KCl. The mycelia were transferred to 20 mL of protoplasting solution (500 mg Driselase [Sigma, D-9515], 200 mg Lysing enzyme [Sigma, L- 1412], and 200 mg Yatalase [TaKaRa Biotech, T017] dissolved in 20 mL of 1.2M KCl). This solution was incubated at 28°C with shaking at 170 rpm and was monitored every 10 min for progression. At 40 min, the protoplasts were separated from the mycelial debris by overlaying the protoplast mixture with trapping buffer (0.6 M Sorbitol, 100 mM Tris-HCl, pH 7.5), followed by centrifugation at 1,500 × *g* for 10 min at 4°C. The protoplast layer was transferred to a new tub and washed three times with 30 mL of 1.2 M KCl with centrifugation at 1,500 × *g* for 10 min at 4°C between washes. The protoplasts were resuspended in 5 mL of 1× STC buffer (1.2M Sorbitol, 10 mM Tris-HCl [pH 8.0], 50 mM $CaCl_2$), yielding a final concentration of 10^7 to 10^8 per mL. Dimethyl sulfoxide (DMSO, 7% final concentration) was added, and aliquots (200 μL) were stored in 1.5 mL tubes at −80°C.

Crispr/Cas9 knockout of *STE3* in *F. graminearum*. The entire coding sequence of *STE3* (NCBI GenBank accession: FGSG_07270) was deleted as described previously (77). Briefly, a dual Cas9-gRNA (guide RNA) was used, where two separate crRNAs (CRISPR RNAs), C1 and C2, were designed to target selected protospacer sequences in the 5′ and the 3′ UTRs of (untranslated regions) *STE3*, respectively (Fig. S1; Table 5). The chop chop tool (https://chopchop.cbu.uib.no) was used to identify the best protospacer adjacent motif (PAM) sites that were recognized by the NGG sequence and were upstream and downstream of the *STE3* start and stop codons, respectively. A BLAST search for the selected protospacer sequences within the *F. graminearum* genome on the ENSEMBL Fungi database (https://fungi.ensembl.org/) was conducted to ensure that they displayed less than 15 base pairs (bp) of identity to any off-target locus in the genome. A selectable marker, hygromycin B (Hyg), was used to replace the STE3 gene in the Cas9 mediated gene deletion. A 1,500 bp segment, spanning a region of the pTrpC promoter and the hygromycin B phosphotransferase (hph) and referred to as the hygromycin repair template, was PCR amplified from the Prf-HU2 vector (78), using a designed primer set, namely, P1 and P2 (Table 1) and Phusion Hotstart polymerase (NEB, M0530S). The resulting PCR fragment was purified using a PCR purification kit (Qiagen, 28104), yielding the complete repair template, which was composed of a Hyg cassette flanked by 50 bp microhomology regions targeting coding regions for the *STE3* gene. The *in vitro* assembly of commercially available, Alt-R-CRISPR-Cas9 components from Integrated DNA Technologies (IDT) was carried out with Cas9 ribonucleoproteins (RNPs), the crRNAs, and tracrRNA (trans-activating CRISPR RNA). The *F. graminearum* strain DAOM 233423 protoplasts were thawed on ice, and 200 μL were transferred to a sterile 15 mL tube that contained the reaction mixture of the dual RNPs targeting the 5′ and 3′ end of the STE3 gene. Approximately 9 μg of the purified hygromycin repair template (150 μL in volume) and 25 μL of polyethylene glycol (PEG)-$CaCl_2$ buffer (60% wt/vol PEG 4000, 50 mM $CaCl_2 \cdot 2H_2O$, 450 mM Tris-HCl, pH 7.5) were added, and the mixture was incubated on ice for 50 min. Subsequently, 1.25 mL of PEG-$CaCl_2$ buffer were added, and the mixture was incubated at room temperature for another 20 min. The mixture was diluted to a total volume of 4 mL via the addition of TB3 molten media (3 g/L yeast extract, 3 g/L Casamino acids, 200 g sucrose/L) and was incubated for 18 h at 25°C at 150 rpm to allow for the regeneration of the fungal cell walls. Finally, 300 μL of the transformed protoplasts were mixed with 15 mL of low melting point agar (Thermo Fisher, 16520050) supplemented with 100 μg/mL hygromycin and spread onto culturing plates. The plates were incubated at 28°C for 4 days, until mycelium emerged from the surface. Putative transformants were picked and subjected to two further rounds of selection on potato dextrose agar (PDA) plates supplemented with 150 μg/mL of hygromycin. Individual colonies were picked, and conidia were obtained by growing in CMC media. The conidia were harvested and stored at −80°C.

Fungal genomic DNA isolation and whole-genome sequencing. Fungal conidia stocks of the transformants at −80°C were thawed on ice and grown in potato dextrose broth (PDB) media. Mycelia were collected from 2-day-old *F. graminearum* liquid cultures by filtration and ground into a fine powder in liquid

nitrogen. Genomic DNA (gDNA) was then isolated from the ground tissue using an E.Z.N.A. Fungal DNA Mini Kit (Omega Biotek, D3390-01) and eluted in sterile water. The deletion of the target *STE3* sequence was confirmed by PCR, using primer set P1 and P2 for the hygromycin gene and P3 and P4 to show the absence of *FgSTE3* (Table 5). *FgSTE3* deletion was validated via whole-genome sequencing performed on a NovaSeq 6000 PE100 (5M reads) platform, following Illumina shotgun library preparation. The FASTQ files were uploaded and the data were analyzed using the Qiagen CLC-Genomics platform (v. 21.0.5), using the default settings. In brief, reads with an error probability of <0.05 (corresponding to a Phred score of $\sim$15) and with more than 2 ambiguous bases were trimmed. Terminal nucleotides were trimmed by 10 bases from the 5′ end to limit sequencing bias, and IDT dual-index sequencing adaptors were removed, resulting in an average read length of 90.8 bases. The trimmed sequences were aligned to the reference genome (GCA_023242275.1) using the "Map Reads to Reference" tool in the CLC-Genomics Workbench with the default settings, resulting in a 90.5% mapping efficiency to the reference and an average coverage of 308.95-fold. In total, 3,366 positions in the reference genome (0.009%) were covered by no sequencing reads, including the 1,790 bp corresponding to the region of *FGSG_07270* (i.e., *FgSTE3*).

Quantitative chemotropism plate assays. Chemotropism plate assays were set up as described previously with minor modifications (24). Chemoattractant solutions (50 μL) that included either 4 μM horseradish peroxidase (HRP; Sigma, P8375) in water or 378 μM chemically synthesized (Bio Basics) *F. graminearum* a-factor (QKPGYPLSCTVM) or α-factor pheromones (WCTWKGQPCW) dissolved in 50% methanol (vol/vol) were loaded in plate wells against solvent controls (water or 50% methanol [vol/vol], respectively). The plates were incubated at 28°C in the dark for 14 h. The directional growth of conidial germ tubes (hyphal tips) was quantified with a stereomicroscope (ZEISS Axiocam ERc 5s). The chemotropic index calculations were obtained using the formula $[N_{test} - N_{solv}]/(N_{total}) \times 100$, where N_{test} is the number of hyphae growing toward the chemoattractant solutions, N_{solv} is the number of hyphae growing toward the solvent control, and N_{total} is the total number of hyphae counted. For each interaction, a minimum of 500 hyphal tips were scored. The plotted data are the averages of 3 independent biological replicates (n = 500 hyphae/interaction/replicate; **, $P < 0.001$). The statistical analysis was conducted using Student's t test.

Wheat coleoptile infection assay. The infection of germinating coleoptiles with the wild-type and *Fgste3Δ3* strains was carried out as previously described (24). Briefly, 16 *Triticum aestivum* cultivar "Roblin" seeds per *F. graminearum* strain to be tested were placed on 1/2 MS media in 0.7% (wt/vol) agar in water in autoclaved Magenta boxes and were stratified overnight at 4°C in the dark. The Magenta boxes were then placed in a growth chamber (Enconair chamber AC 60) with growth light and temperature conditions set to 20°C day and 16°C night, with a 16 h photoperiod (750 μmol photons/m^2·s), and coleoptiles were grown to a height of 1 cm, with 12 to 16 seeds germinated per strain. Sterile scissors were used to cut 1 mm off the top of the coleoptile, and cotton thread soaked in a macro conidial suspension (2×10^5 conidia per mL) was wrapped around the wound site. The Magenta boxes were then placed back into the growth chamber to allow for symptom development. After 10 days, the lengths of the infected lesions observed on the coleoptile stalks were measured for each strain. The averages of two independent biological replicate experiments are shown (compared to the wild-type strain; n = 18 for each experiment). The statistical analysis was conducted using a one-way analysis of variance (ANOVA).

***A. thaliana* detached leaf assay with fungal biomass quantification.** Conidia concentrations for the wild-type and knockout strains were adjusted to 1×10^4 conidia/mL. Briefly, 10 detached leaves from 3-week old *A. thaliana* Col-0 plants were transferred onto a petri-plate containing 1% agar. Wound inoculation on detached leaves of *A. thaliana* was conducted as previously described (79, 80). Plates were incubated in the dark at 28°C to simulate the conditions required for infection. The progression of disease and lesion development on leaves were monitored for 3 days. Fungal DNA isolation from *A. thaliana* leaves at 2-days postinfection was performed using a Phytopure plant DNA extraction kit, according to the manufacturer's instructions (Amersham Biosciences, QC, Canada). DNA (30 ng) was applied to qPCR using PowerUP Syber Green Master Mix (Applied Biosystems). Primers of the fungal rDNA-ITS region (P5 and P6) and *A. thaliana* PP2A (AT1G69960; P7 and P8) were used for normalization to calculate the relative expression levels (Table 1). Two biological replicate experiments were averaged (n = 12 each) for the leaf assay, and 3 biological replicates were averaged for the qPCR assay.

Wheat head infection assay. A pathology test was performed by point inoculation on a susceptible variety of wheat (*cv.* Roblin) (81). Two independent biological repetition experiments were performed with 11 to 15 wheat spikelets per experiment.

DON quantification. Deoxynivalenol production was measured *in vitro* using a modified two-stage media protocol (81). Briefly, 5,000 conidia/mL were inoculated into 4 mL of 95% putrescine second-stage media (6.2 mM Putrescine di-hydrochloride, 22 mM KH_2PO_4, 0.8 mM $MgSO_4 \cdot 7H_2O$, 85.6 mM NaCl, 116.8 mM sucrose, 108.6 mM glycerol [vol/vol], pH 4.0), and 5% glucose yeast-extract peptone first-stage media (GYEP; 56 mM NH_4Cl, 8.1 mM $MgSO_4$ $7H_2O$, 0.23 mM $FeSO_4 \cdot 7H_2O$, 14.7 mM KH_2PO_4, 2 g/L peptone, 2 g/L yeast extract, 2 g/L malt extract, and 111 mM glucose) per well, with each containing one sterile nylon filter (Millipore #NY1H). Culture plates were incubated at 28°C and 160 rpm in the dark for 72 h. Mycelia were vacuum-dried and weighed. Culture supernatants were filtered (0.2 μM) and diluted to a final concentration of 15% MeOH. Trichothecenes were analyzed on a Shimadzu Prominence LC-20AD (Mandel) with a 100 μL injection on a Shimadzu SIL-20A HT Prominence autosampler. Samples were run using a 22.5% isocratic methanol:water mobile phase at a rate of 1 mL/min for 20 min on a Restek Pinnacle DB C18 column (5uM, 150 $\times$ 4.6 mm, Cat. number 9414565). Trichothecenes (DON) were monitored by UV at 220 nm and were reported as micrograms of toxin per milligram of mycelial tissue.

Western blotting of MAPKs. Approximately 10^5 *F. graminearum* conidia for each respective strain were grown in PDB for 24 h at 28°C in the dark. HRP (0.05 μM) or an equivalent water control was then added to the growing culture and shaken for 1 h. The cells were lysed as previously described (82). The total protein (20 μg) of each sample was loaded and resolved on a 12% SDS polyacrylamide gel and transferred to a polyvinylidene difluoride membrane (PVDF, Bio-Rad) via wet electroblotting at 100 V for 2 h. The membranes were blocked for 1 h in 5% (wt/vol) nonfat, dried, skim milk in TBST buffer (50 mM Tris [pH 7.5], 150 mM NaCl, 0.05% [vol/vol] Tween 20) at 4°C. The membranes were subsequently incubated with either anti-p44/42 MAP kinase (1:1,000 dilution, M5670, Millipore Sigma) or anti-phospho p44/42 MAP kinase (1:1,000 dilution, Cell Signaling Technology, 9101) primary antibodies. Following a wash step, the membranes were incubated with HRP linked IgG secondary antibody for 1 h at room temperature for chemiluminescent detection (1:5,000 dilution, Cell Signal Technology, 7074S). For visualization, enhanced chemiluminescent substrate (Thermo Scientific, 32209) was added to the membranes, and the emitted light was captured using a GelDoc Imager and the Image Lab software package (Bio-Rad). The membrane was stripped and then re-probed for α-tubulin (1:1000, Santa Cruz Biotechnology, sc53030) as a loading control. Quantification was performed using ImageJ (83) (https://imagej.nih.gov/ij/, 1997 to 2018). Three independent biological repetitions of the experiment were averaged and analyzed using Student's *t* test.

Total RNA extraction and differential RNA-Seq analysis. Approximately 2×10^5 conidia of both the wild-type and the *Fgste3Δ-3* strains were grown in 2 × 20 mL of PDB for 3 days at 28°C in the dark. At this time, one culture of each strain type was induced with 0.05 μM HRP, whereas the other was left to grow uninduced. After a further 24 h, the mycelia from all of the cultures were harvested. For RNA extraction, 1 g of dried mycelial mass was frozen in liquid nitrogen and homogenized in 1 mL of TRIzol reagent, prepared according to the manufacturer's instructions (Thermo Fisher Scientific). The InviTrap Spin Universal RNA Mini Kit (Stratec Molecular, Germany) was used to purify the total RNA from the TRIzol aqueous phase, according to the manufacturer's protocol. The RNA concentration and purity were subsequently determined using a Nanodrop spectrophotometer ND-1000 (Thermo Scientific). The RNA-Seq libraries were prepared using a TruSeq Stranded RNALT Kit and were sequenced on an Illumina HiSeq 2500 platform, according to the manufacturer's guidelines (Illumina, USA). The *F. graminearum* RNA-Seq data were analyzed using CLC Genomics Workbench, version 11.0.1 (Qiagen Corp.). The raw data were trimmed using Trimmomatic v0.39 (http://www.usadellab.org/cms/?page=trimmomatic), based on the default quality scores that were determined by the base caller error probability level ($P < 0.01$). To estimate the expression levels, high quality RNA sequences were aligned to the *F. graminearum* RR1.36 genome that was annotated with genes and transcripts using Salmon v1.2.1 (https://combine-lab.github.io/salmon/) (84). A differential expression analysis was performed using SARTools v1.6.4 with the DESeq2 option and the parameters provided within the default template (85). The differentially expressed transcripts over the threshold false discovery rate (FDR) (86) of corrected adjusted *P* values of ≤0.05 were considered. Gene annotation and a GO enrichment analysis for *F. graminearum* were accomplished within the FungiDB database (https://fungidb.org/fungidb/) (87, 88) and the KOBAS database (http://kobas.cbi.pku.edu.cn) (89). The full RNA-Seq data set is available from the NCBI (Bioproject ID: PRJNA872394). Three biological replicates were used per condition.

SUPPLEMENTAL MATERIAL

Supplemental material is available online only.

DATA SET S1, XLSX file, 0.4 MB.

FIG S1, TIF file, 0.7 MB.

FIG S2, TIF file, 1.2 MB.

FIG S3, TIF file, 1 MB.

FIG S4, TIF file, 1.3 MB.

FIG S5, TIF file, 1.5 MB.

FIG S6, TIF file, 2.4 MB.

ACKNOWLEDGMENTS

T.S. planned and carried out most of the experiments, analyzed and interpreted the data, and wrote the first draft of the paper. P.S. performed the coleoptile assays. C.B performed the pathology assays and interpreted the whole-genome sequencing results. S.F. processed the transcriptomic data. G.S helped plan the CRISPR experiment and the pathology assays and interpreted the results. J.S.A. designed the experiments and interpreted the results. M.C.L. conceived the idea, obtained the funding, oversaw the planning of experiments, interpreted the data, and helped write the final version of the paper. All coauthors edited the manuscript.

We declare no competing interests.

This work was funded by Discovery Grants from the Natural Sciences and Engineering Research Council to both J.S.A. (# 356025–2019) and M.C.L (# 261683–2018) as well as by the National Research Council of Canada to M.C.L.

REFERENCES

1. Brand A, Gow NA. 2009. Mechanisms of hypha orientation of fungi. Curr Opin Microbiol 12:350–357. https://doi.org/10.1016/j.mib.2009.05.007.
2. Shi C, Kaminskyj S, Caldwell S, Loewen MC. 2007. A role for a complex between activated G protein-coupled receptors in yeast cellular mating. Proc Natl Acad Sci U S A 104:5395–5400. https://doi.org/10.1073/pnas.0608219104.
3. Alvaro CG, Thorner J. 2016. Heterotrimeric G protein-coupled receptor signaling in yeast mating pheromone response. J Biological Chemistry 291:7788–7795. https://doi.org/10.1074/jbc.R116.714980.
4. Jackson CL, Konopka JB, Hartwell LHS. 1991. *Saccharomycese cerevisiae* alpha pheromone receptors activate a novel signal transduction pathway for mating partner discrimination. Cell 67:389–402. https://doi.org/10.1016/0092-8674(91)90190-A.
5. Haber JE. 2012. Mating-type genes and MAT switching in *Saccharomyces cerevisiae*.
6. Jones SK, Bennett RJ. 2011. Fungal mating pheromones: choreographing the dating game. Fungal Genet Biol 48:668–676. https://doi.org/10.1016/j.fgb.2011.04.001.
7. Dube P, Konopka JB. 1998. Identification of a polar region in transmembrane domain 6 that regulates the function of the G protein-coupled alpha-factor receptor. Mol Cell Biol 18:7205–7215. https://doi.org/10.1128/MCB.18.12.7205.
8. Schrick K, Garvik B, Hartwell LH. 1997. Mating in *Saccharomyces cerevisiae*: the role of the pheromone signal transduction pathway in the chemotropic response to pheromone. Genetics 147:19–32. https://doi.org/10.1093/genetics/147.1.19.
9. Segall JE. 1993. Polarization of yeast cells in spatial gradients of α mating factor. Proc Natl Acad Sci U S A 90:8332–8336. https://doi.org/10.1073/pnas.90.18.8332.
10. Manavathu EK, Thomas DS. 1985. Chemotropism of *Achlya ambisexualis* to methionine and methionyl. Microbiology (N Y)131:751–756. https://doi.org/10.1099/00221287-131-4-751.
11. Jones SW, Donaldson SP, Deacon JW. 1991. Behaviour of zoospores and zoospore cysts in relation to root infection by *Pythium aphanidermatum*. New Phytol 117:289–301. https://doi.org/10.1111/j.1469-8137.1991.tb04910.x.
12. Musgrave A, Ero L, Scheffer R, Oehlers E. 1977. Chemotropism of *Achlya bisexualis* germ hyphae to casein hydrolysate and amino acids. J Gen Microbiol 101:65–70. https://doi.org/10.1099/00221287-101-1-65.
13. Jansson H-B, Johansson T, Nordbring-Hertz B, Tunlid A, Odham G. 1988. Chemotropic growth of germ-tubes of *Cochliobolus sativus* to barley roots or root exudates. Transactions of the British Mycological Society 90:647–650. https://doi.org/10.1016/S0007-1536(88)80072-X.
14. Zentmyer GA. 1961. Chemotaxis of zoospores for root exudates. Science 133:1595–1596. https://doi.org/10.1126/science.133.3464.1595.
15. Turrà D, el Ghalid M, Rossi F, di Pietro A. 2015. Fungal pathogen uses sex pheromone receptor for chemotropic sensing of host plant signals. Nature 527:521–524. https://doi.org/10.1038/nature15516.
16. Brown NA, Schrevens S, van Dijck P, Goldman GH. 2018. Fungal G-protein-coupled receptors: mediators of pathogenesis and targets for disease control. Nat Microbiol 3:402–414. https://doi.org/10.1038/s41564-018-0127-5.
17. Jiang C, Cao S, Wang Z, Xu H, Liang J, Liu H, Wang G, Ding M, Wang Q, Gong C, Feng C, Hao C, Xu JR. 2019. An expanded subfamily of G-protein-coupled receptor genes in *Fusarium graminearum* required for wheat infection. Nat Microbiol 4:1582–1591. https://doi.org/10.1038/s41564-019-0468-8.
18. Lottersberger F, Panza A, Lucchini G, Piatti S, Longhese MP. 2006. The *Saccharomyces cerevisiae* 14–3-3 proteins are required for the G1/S transition, actin cytoskeleton organization and cell wall integrity. Genetics 173:661–675. https://doi.org/10.1534/genetics.106.058172.
19. El-Defrawy MMH, El-Latif Hesham A. 2020. G-protein-coupled receptors in fungi, *In* Fungal Biotechnology and Bioengineering (Hesham AL, Upadhyay R, Sharma G, Manoharachary C, Gupta V., ed), pp 37–126. Springer, Cham.
20. Leberer E, Thomas DY, Whiteway M. 1997. Pheromone signalling and polarized morphogenesis in yeast. Curr Opin Genet Dev 7:59–66. https://doi.org/10.1016/S0959-437X(97)80110-4.
21. Martin SH, Wingfield BD, Wingfield MJ, Steenkamp ET. 2011. Causes and consequences of variability in peptide mating pheromones of ascomycete fungi. Mol Biol Evol 28:1987–2003. https://doi.org/10.1093/molbev/msr022.
22. Vitale S, di Pietro A, Turrà D. 2019. Autocrine pheromone signalling regulates community behaviour in the fungal pathogen *Fusarium oxysporum*. Nat Microbiol 4:1443–1449. https://doi.org/10.1038/s41564-019-0456-z.
23. Vangalis V, Markakis EA, Knop M, di Pietro A, Typas MA, Papaioannou IA. 2022. Components of kinase signaling control chemotropism and pathogenicity in the fungal pathogen *Verticillium dahliae*. BioRxiv:496898.
24. Sridhar PS, Trofimova D, Subramaniam R, González-Peña Fundora D, Foroud NA, Allingham JS, Loewen MC. 2020. Ste2 receptor-mediated chemotropism of *Fusarium graminearum* contributes to its pathogenicity against wheat. Sci Rep 10:10770. https://doi.org/10.1038/s41598-020-67597-z.
25. Martínez-Soto D, Ruiz-Herrera J. 2017. Functional analysis of the MAPK pathways in fungi. Rev Iberoam Micol 34:192–202. https://doi.org/10.1016/j.riam.2017.02.006.
26. Wanjiru WM, Zhensheng K, Buchenauer H. 2002. Importance of cell wall degrading enzymes produced by *Fusarium graminearum* during infection of wheat heads. Eur J Plant Pathol 108:803–810. https://doi.org/10.1023/A:1020847216155.
27. Zheng D, Zhang S, Zhou X, Wang C, Xiang P, Zheng Q, Xu JR. 2012. The FgHOG1 Pathway regulates hyphal growth, stress responses, and plant infection in *Fusarium graminearum*. PLoS One 7:e49495. https://doi.org/10.1371/journal.pone.0049495.
28. Kim HK, Lee T, Yun SH. 2008. A putative pheromone signaling pathway is dispensable for self-fertility in the homothallic ascomycete *Gibberella zeae*. Fungal Genet Biol 45:1188–1196. https://doi.org/10.1016/j.fgb.2008.05.008.
29. Lee J, Leslie JF, Bowden RL. 2008. Expression and function of sex pheromones and receptors in the homothallic ascomycete *Gibberella zeae*. Eukaryot Cell 7:1211–1221. https://doi.org/10.1128/EC.00272-07.
30. Bresso E, Togawa R, Hammond-Kosack K, Urban M, Maigret B, Martins NF. 2016. GPCRs from *Fusarium graminearum* detection, modeling and virtual screening - the search for new routes to control head blight disease. BMC Bioinformatics 17:39–52. https://doi.org/10.1186/s12859-016-1342-9.
31. Zhang XW, Jia LJ, Zhang Y, Jiang G, Li X, Zhang D, Tang WH. 2012. In planta stage-specific fungal gene profiling elucidates the molecular strategies of *Fusarium graminearum* growing inside wheat coleoptiles. Plant Cell 24:5159–5176. https://doi.org/10.1105/tpc.112.105957.
32. Boenisch MJ, Schäfer W. 2011. *Fusarium graminearum* forms mycotoxin producing infection structures on wheat. BMC Plant Biol 11:110–114. https://doi.org/10.1186/1471-2229-11-110.
33. O'Mara SP, Broz K, Dong Y, Kistler HC. 2021. The *Fusarium graminearum* transporters Abc1 and Abc6 are important for xenobiotic resistance, trichothecene accumulation, and virulence to wheat. bioRxiv. 2021.06.15.448535.
34. Wang SC, Davejan P, Hendargo KJ, Javadi-Razaz I, Chou A, Yee DC, Ghazi F, Lam KJK, Conn AM, Madrigal A, Medrano-Soto A, Saier MH. 2020. Expansion of the major facilitator superfamily (MFS) to include novel transporters as well as transmembrane-acting enzymes. Biochim Biophys Acta Biomembr 1862:183277. https://doi.org/10.1016/j.bbamem.2020.183277.
35. Stolz J, Caspari T, Carr AM, Sauer N. 2004. Cell division defects of *Schizosaccharomyces pombe* liz1− mutants are caused by defects in pantothenate uptake. Eukaryot Cell 3:406–412. https://doi.org/10.1128/EC.3.2.406-412.2004.
36. Ene I. v, Walker LA, Schiavone M, Lee KK, Martin-Yken H, Dague E, Gow NAR, Munro CA, Brown AJP. 2015. Cell wall remodeling enzymes modulate fungal cell wall elasticity and osmotic stress resistance. mBio 6:e00986-15. https://doi.org/10.1128/mBio.00986-15.
37. Dalto M, Daniels J. 2017. Fungi. *Practical Handbook of Microbiology, Third Edition* 937–962.
38. Hurley JH. 1996. The sugar kinase/heat shock protein 70/actin superfamily: implications of conserved structure for mechanism. Annu Rev Biophys Biomol Struct 25:137–162. https://doi.org/10.1146/annurev.bb.25.060196.001033.
39. Nordzieke DE, Fernandes TR, el Ghalid M, Turrà D, di Pietro A. 2019. NADPH oxidase regulates chemotropic growth of the fungal pathogen *Fusarium oxysporum* towards the host plant. New Phytol 224:1600–1612. https://doi.org/10.1111/nph.16085.
40. Ding Y, Gardiner DM, Xiao D, Kazan K. 2019. Novel regulators of nitric oxide signaling triggered by host perception in a plant pathogen. bioRxiv:779173.
41. van Dyck L, Dembowski M, Neupert W, Langer T. 1998. Mcx1p, a ClpX homologue in mitochondria of *Saccharomyces cerevisiae*. FEBS Lett 438:250–254. https://doi.org/10.1016/S0014-5793(98)01310-6.
42. Ibrahim YM, Kerr AR, Silva NA, Mitchell TJ. 2005. Contribution of the ATP-dependent protease ClpCP to the autolysis and virulence of *Streptococcus pneumoniae*. Infect Immun 73:730–740. https://doi.org/10.1128/IAI.73.2.730-740.2005.
43. Frees D, Qazi SNA, Hill PJ, Ingmer H. 2003. Alternative roles of ClpX and ClpP in *Staphylococcus aureus* stress tolerance and virulence. Mol Microbiol 48:1565–1578. https://doi.org/10.1046/j.1365-2958.2003.03524.x.

44. Goodman AL, Merighi M, Hyodo M, Ventre I, Filloux A, Lory S. 2009. Direct interaction between sensor kinase proteins mediates acute and chronic disease phenotypes in a bacterial pathogen. Genes Dev 23:249–259. https://doi.org/10.1101/gad.1739009.
45. Davies JA, Harrison JJ, Marques LLR, Foglia GR, Stremick CA, Storey DG, Turner RJ, Olson ME, Ceri H. 2007. The GacS sensor kinase controls phenotypic reversion of small colony variants isolated from biofilms of *Pseudomonas aeruginosa* PA14. FEMS Microbiol Ecol 59:32–46. https://doi.org/10.1111/j.1574-6941.2006.00196.x.
46. Tanaka S, Nojima H. 1996. Nik1: a Nim1-like protein kinase of *S. cerevisiae* interacts with the Cdc28 complex and regulates cell cycle progression. Genes Cells 1:905–921. https://doi.org/10.1046/j.1365-2443.1996.d01-213.x.
47. Prado-Cabrero A, Scherzinger D, Avalos J, Al-Babili S. 2007. Retinal biosynthesis in fungi: characterization of the carotenoid oxygenase CarX from *Fusarium fujikuroi*. Eukaryot Cell 6:650–657. https://doi.org/10.1128/EC.00392-06.
48. Buhrow LM, Cram D, Tulpan D, Foroud NA, Loewen MC. 2016. Exogenous abscisic acid and gibberellic acid elicit opposing effects on *Fusarium graminearum* infection in wheat. Phytopathology 106:88.
49. Buhrow LM, Liu Z, Cram D, Sharma T, Foroud NA, Pan Y, Loewen MC. 2021. Wheat transcriptome profiling reveals abscisic and gibberellic acid treatments regulate early-stage phytohormone defense signaling, cell wall fortification, and metabolic switches following *Fusarium graminearum*-challenge. BMC Genomics 22:798. https://doi.org/10.1186/s12864-021-08069-0.
50. Falter C, Reumann S. 2022. The essential role of fungal peroxisomes in plant infection. Mol Plant Pathol 00:1–14.
51. Wu PC, Chen YK, Yago JI, Chung KR. 2021. Peroxisomes implicated in the biosynthesis of siderophores and biotin, cell wall integrity, autophagy, and response to hydrogen peroxide in the citrus pathogenic fungus *Alternaria alternata*. Front Microbiol 12:1588.
52. Zhang D, Dailey OR, Simon DJ, Roca-Datzer K, Jami-Alahmadi Y, Hennen MS, Wohlschlegel JA, Koehler CM, Dabir Dv. 2021. Aim32 is a dual-localized 2Fe-2S mitochondrial protein that functions in redox quality control. J Biol Chem 297:101135. https://doi.org/10.1016/j.jbc.2021.101135.
53. Black B, Lee C, Horianopoulos LC, Jung WH, Kronstad JW. 2021. Respiring to infect: emerging links between mitochondria, the electron transport chain, and fungal pathogenesis. PLoS Pathog 17:e1009661. https://doi.org/10.1371/journal.ppat.1009661.
54. Verma S, Shakya VPS, Idnurm A. 2018. Exploring and exploiting the connection between mitochondria and the virulence of human pathogenic fungi. Virulence 9:426–446. https://doi.org/10.1080/21505594.2017.1414133.
55. Liu X, Han Q, Wang J, Wang X, Xu J, Shi J. 2016. Two FgLEU2 genes with different roles in leucine biosynthesis and infection-related morphogenesis in *Fusarium graminearum*. PLoS One 11:e0165927. https://doi.org/10.1371/journal.pone.0165927.
56. Liu X, Han Q, Xu J, Wang J, Shi J. 2015. Acetohydroxyacid synthase FgIlv2 and FgIlv6 are involved in BCAA biosynthesis, mycelial and conidial morphogenesis, and full virulence in *Fusarium graminearum*. Sci Rep 5:16315. https://doi.org/10.1038/srep16315.
57. Sieber CMK, Lee W, Wong P, Münsterkötter M, Mewes H-W, Schmeitzl C, Varga E, Berthiller F, Adam G, Güldener U. 2014. The *Fusarium graminearum* genome reveals more secondary metabolite gene clusters and hints of horizontal gene transfer. PLoS One 9:e110311. https://doi.org/10.1371/journal.pone.0110311.
58. Kou Y, Tan YH, Ramanujam R, Naqvi NI. 2017. Structure-function analyses of the Pth11 receptor reveal an important role for CFEM motif and redox regulation in rice blast. New Phytol 214:330–342. https://doi.org/10.1111/nph.14347.
59. Fredriksson R, Schiöth HB. 2005. The repertoire of G-protein-coupled receptors in fully sequenced genomes. Mol Pharmacol 67:1414–1425. https://doi.org/10.1124/mol.104.009001.
60. Natarajan SK, Muthukrishnan E, Khalimonchuk O, Mott JL, Becker DF. 2017. Evidence for pipecolate oxidase in mediating protection against hydrogen peroxide stress. J Cell Biochem 118:1678–1688. https://doi.org/10.1002/jcb.25825.
61. Seifert R, Wenzel-Seifert K. 2002. Constitutive activity of G-proteins-coupled receptors: cause of disease and common property of wild-type receptors. Naunyn Schmiedebergs Arch Pharmacol.
62. Rocha ALM, di Pietro A, Ruiz-Roldán C, Roncero MIG. 2008. Ctf1, a transcriptional activator of cutinase and lipase genes in *Fusarium oxysporum* is dispensable for virulence. Mol Plant Pathol 9:293–304. https://doi.org/10.1111/j.1364-3703.2007.00463.x.
63. Rerngsamran P, Murphy MB, Doyle SA, Ebbole DJ. 2005. Fluffy, the major regulator of conidiation in *Neurospora crassa*, directly activates a developmentally regulated hydrophobin gene. Mol Microbiol 56:282–297. https://doi.org/10.1111/j.1365-2958.2005.04544.x.
64. Cohrs KC, Schumacher J. 2017. The two cryptochrome/photolyase family proteins fulfill distinct roles in DNA photorepair and regulation of conidiation in the gray mold fungus *Botrytis cinerea*. Appl Environ Microbiol 83. https://doi.org/10.1128/AEM.00812-17.
65. Carmen Ruiz-Roldán M, Garre V, Guarro J, Mariné M, Isabel M, Roncero G. 2008. Role of the white collar 1 photoreceptor in carotenogenesis, UV resistance, hydrophobicity, and virulence of *Fusarium oxysporum*. Eukaryot Cell 7:1227–1230. https://doi.org/10.1128/EC.00072-08.
66. Cuperlovic-Culf M, Loewen M, Rajagopalan N, Surendra A. 2017. Perspectives on the specific targeting of *Fusarium graminearum* for the development of alternative head blight treatment approaches. Plant Pathol 66:1391–1403. https://doi.org/10.1111/ppa.12726.
67. Rampitsch C, Leung WWY, Blackwell BA, Subramaniam R. 2011. MAP kinase Mgv1: A potential shared control point of butenolide and deoxynivalenol biosynthesis in *Fusarium graminearum*. Plant Breed Seed Sci 54:81–88.
68. Ren J, Li C, Gao C, Xu J-R, Jiang C, Wang G. 2019. Deletion of FgHOG1 is suppressive to the mgv1 mutant by stimulating Gpmk1 activation and avoiding intracellular turgor elevation in *Fusarium graminearum*. Front Microbiol 10.
69. Dale N. C, Johnstone EKM, Pfleger KDG. 2022. GPCR heteromers: an overview of their classification, function and physiological relevance. Front Endocrinol (Lausanne) Frontiers Media S.A.
70. Shi C, Paige MF, Maley J, Loewen MC. 2009. *In vitro* characterization of ligand-induced oligomerization of the *S. cerevisiae* G-protein coupled receptor, Ste2p. Biochim Biophys Acta 1790:1–7. https://doi.org/10.1016/j.bbagen.2008.10.003.
71. Thaler JS, Humphrey PT, Whiteman NK. 2012. Evolution of jasmonate and salicylate signal crosstalk. Trends Plant Sci 17:260–270. https://doi.org/10.1016/j.tplants.2012.02.010.
72. Di X, Gomila J, Takken FLW. 2017. Involvement of salicylic acid, ethylene and jasmonic acid signalling pathways in the susceptibility of tomato to *Fusarium oxysporum*. Mol Plant Pathol 18:1024–1035. https://doi.org/10.1111/mpp.12559.
73. Goodman JL, Wang S, Alam S, Ruzicka FJ, Frey PA, Wedekind JE. 2004. Ornithine cyclodeaminase: structure, mechanism of action, and implications for the mu-crystallin family. Biochemistry 43:13883–13891. https://doi.org/10.1021/bi048207i.
74. Brown NA, Evans J, Mead A, Hammond-Kosack KE. 2017. A spatial temporal analysis of the *Fusarium graminearum* transcriptome during symptomless and symptomatic wheat infection. Mol Plant Pathol 18:1295–1312. https://doi.org/10.1111/mpp.12564.
75. Lamb C, Dixon RA. 1997. The oxidative burst in plant disease resistance. Annu Rev Plant Physiol Plant Mol Biol 48:251–275. https://doi.org/10.1146/annurev.arplant.48.1.251.
76. Perez P, Rincón SA. 2010. Rho GTPases: regulation of cell polarity and growth in yeasts. Biochem J 426:243–253. https://doi.org/10.1042/BJ20091823.
77. Al Abdallah Q, Ge W, Fortwendel JR. 2017. A simple and universal system for gene manipulation in *Aspergillus fumigatus*: in vitro-assembled Cas9-guide RNA ribonucleoproteins coupled with microhomology repair templates. mSphere 2:e00446-17. https://doi.org/10.1128/mSphere.00446-17.
78. Frandsen RJN, Andersson JA, Kristensen MB, Giese H. 2008. Efficient four fragment cloning for the construction of vectors for targeted gene replacement in filamentous fungi. BMC Mol Biol 9:70. https://doi.org/10.1186/1471-2199-9-70.
79. Koch A, Khalifa W, Langen G, Vilcinskas A, Kogel KH, Imani J. 2012. The antimicrobial peptide thanatin reduces fungal infections in *Arabidopsis*. J Phytopathology 160:606–610. https://doi.org/10.1111/j.1439-0434.2012.01946.x.
80. Koch A, Kumar N, Weber L, Keller H, Imani J, Kogel KH. 2013. Host-induced gene silencing of cytochrome P450 lanosterol C14α-demethylase-encoding genes confers strong resistance to *Fusarium* species. Proc Natl Acad Sci U S A 110:19324–19329. https://doi.org/10.1073/pnas.1306373110.
81. Walkowiak S, Bonner CT, Wang L, Blackwell B, Rowland O, Subramaniam R. 2015. Intraspecies interaction of *Fusarium graminearum* contributes to reduced toxin production and virulence. Mol Plant Microbe Interact 28:1256–1267. https://doi.org/10.1094/MPMI-06-15-0120-R.
82. Yun Y, Liu Z, Yin Y, Jiang J, Chen Y, Xu JR, Ma Z. 2015. Functional analysis of the *Fusarium graminearum* phosphatome. New Phytol 207:119–134. https://doi.org/10.1111/nph.13374.
83. Schneider CA, Rasband WS, Eliceiri KW. 2012. NIH image to ImageJ: 25 years of image analysis. Nat Methods 9:671–675. https://doi.org/10.1038/nmeth.2089.
84. King R, Urban M, Hammond-Kosack MCU, Hassani-Pak K, Hammond-Kosack KE. 2015. The completed genome sequence of the pathogenic

ascomycete fungus *Fusarium graminearum*. BMC Genomics 16:1–21. https://doi.org/10.1186/s12864-015-1756-1.
85. Varet H, Brillet-Guéguen L, Coppée JY, Dillies MA. 2016. SARTools: a DESeq2- and EdgeR-based R pipeline for comprehensive differential analysis of RNA-Seq data. PLoS One 11:e0157022. https://doi.org/10.1371/journal.pone.0157022.
86. Benjamini Y, Hochberg Y. 1995. Controlling the false discovery rate: a practical and powerful approach to multiple testing. J R Stat Soc: Series B (Methodological) 57:289–300.
87. Basenko EY, Pulman JA, Shanmugasundram A, Harb OS, Crouch K, Starns D, Warrenfeltz S, Aurrecoechea C, Stoeckert CJ, Kissinger JC, Roos DS, Hertz-Fowler C. 2018. FungiDB: an integrated bioinformatic resource for fungi and oomycetes. JoF 4:39. https://doi.org/10.3390/jof4010039.
88. Stajich JE, Harris T, Brunk BP, Brestelli J, Fischer S, Harb OS, Kissinger JC, Li W, Nayak V, Pinney DF, Stoeckert CJ, Roos DS. 2012. FungiDB: an integrated functional genomics database for fungi. Nucleic Acids Res 40:D675–D681. https://doi.org/10.1093/nar/gkr918.
89. Bu D, Luo H, Huo P, Wang Z, Zhang S, He Z, Wu Y, Zhao L, Liu J, Guo J, Fang S, Cao W, Yi L, Zhao Y, Kong L. 2021. KOBAS-i: intelligent prioritization and exploratory visualization of biological functions for gene enrichment analysis. Nucleic Acids Res 49:W317–W325. https://doi.org/10.1093/nar/gkab447.